NATIONAL AERONAUTICS AND SPACE ADMINISTRATION

Research Grant NGR-09-005-025

Diagnostics of Accelerating Plasma

2nd Semi-Annual Progress Report

September 1, 1966 - February 28, 1967

Report No. 66-021

by

T. N. Lie, A. W. Ali, E. A. McLean

and

C. C. Chang

February 28, 1967

Department of Space Science and Applied Physics
The Catholic University of America
Washington, D.C. 20017

ABSTRACT

The radial electron density distributions, the electron temperatures, and the shapes of the current sheets produced in coaxial plasma accelerators of different radius ratio were determined using fast photography and spectroscopic techniques. Pronounced polarity effect in these accelerators were observed for most of the working gases used. However, in the case of hydrogen the polarity dependent behavior is much less noticeable. Present experimental methods were extended to the discharge plasma produced in a parallel plate plasma accelerator in an attempt to gain better understanding on the current sheet behavior.

Since some of the spectroscopic techniques used or to be used in the investigation depend on the assumption of local thermal equilibrium, the validity of LTE in the plasma under interest was studied and its theoretical result is given.

TABLE OF CONTENTS

LIST OF ILLUSTRATIONS

I. Introduction

In the previous semi-annual report, some of the quantitative measurements on plasma properties of the current sheet produced in a coaxial plasma accelerator were given. The same experimental methods have been extended to coaxial accelerators of different radius ratio and to an accelerator filled with various species of working gases. Section I describes the polarity-dependent behavior of the current sheet produced in the coaxial accelerators. It is shown that the polarity effect in the electron density distributions, the electron temperatures, and in the shape of the current sheet is a distinct phenomena regardless of its geometry or the species of the working gas used. However, in the case of hydrogen, the difference between the two opposite polarity cases was less distinct.

The polarity effect may be caused by the fact that there is a different behavior of the current sheet near the positive and the negative electrode. This problem may be studied somewhat easier by using the sheet produced in a parallel-plate plasma accelerator with the present experimental techniques. Some of the preliminary results are shown in Section III; however, quantitative measurements are under way which also include radiation losses due to line emission in the vacuum ultra violet region of the spectrum.

Since some of the spectroscopic techniques used in the investigation depend on the assumption of local thermal equilibrium (LTE) in the plasma under interest, the validity of the measurements depends on the assumption of LTE. Section IV describes a comprehensive study of this problem. The collisional and radiative processes which determine the population densities of He III, and various bound states of He II and He I, are examined and it is concluded that the LTE assumption is in fact a satisfactory approximation for the conditions of the current sheet produced in the accelerator.

II. Electric Polarity Effect in a Coaxial Plasma Accelerator

A. Introduction and Description of Accelerator

In general, the behavior of the current sheet in a coaxial plasma accelerator depends on its electric polarity arrangement, the species of the working gas, and the accelerator geometry. The polarity dependence on the discharge current pattern in argon gas has been studied by Keck.[1] However, Lovberg[2] found no significant polarity effect in his hydrogen-filled accelerator and it was suggested that the difference may lie in the use of heavy and light gases. The casue of this effect may be due to the difference in the behavior of the current sheet at the positive and negative electrodes. It has been shown[3], [4], [5] that the current sheet behaves differently near the cathode and anode in the parallel plate plasma accelerator. The objective of the present experimental study is to demonstrate the polarity dependence of the shape, the electron density, and the temperature of the current sheet for several coaxial plasma accelerators of different radius ratio. Spectroscopic techniques for the plasma diagnostics have been used throughout the study.

The dimensions of the accelerators used in the study are shown in Table I. These accelerators were operated in both polarities and the discharge was triggered by a simple three-point spark gap. A coaxial, disc-type capacitor of 10 μF was charged to 9 kV and the ringing frequency of the discharges was about 400 kc/s. For most of the measurements the accelerators were filled with helium to a static ambient pressure of 0.5 Torr prior to the discharge. However, hydrogen, nitrogen and argon were also used as the working gases for qualitative observations.

ACCELERATOR	DIA. of O.E in mm	DIA. of I.E in mm	LENGTH of O.E in mm	LENGTH of I.E in mm	RADIUS RATIO
#1A	50	28	65	120	1.8
#1B	50	16	65	120	3.1
#2B	50	16	100	120	3.1
#1C	50	8	65	120	6.3
#5A	62	28	65	120	2.2
#5D	62	40	65	100	1.5

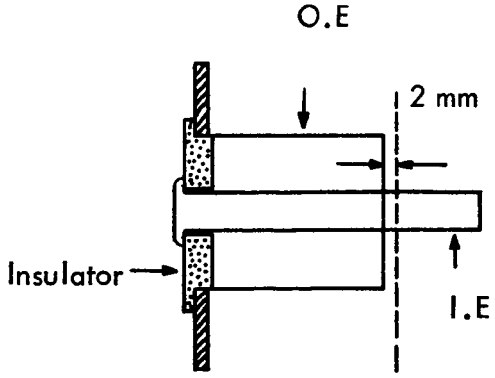

Line of Sight

TABLE 1
DIMENSIONS OF COAXIAL ACCELERATORS

B. Radial Electron Density Distribution

Electron densities were determined from the half-widths of the Stark line profiles of He II 4686 Å. The profiles were plotted on a shot-to-shot basis, assuming reproducibility of the discharge. The measurements were taken at three locations in the radial plane which is perpendicular to the accelerator axis and separated by 2 mm from the outer electrode end. The sources of error in the measurements are:

1) lack of detailed reproducibility of the discharge,

2) non-uniform density configuration along the line of sight, and

3) errors due to the theoretical treatment (6) of the Stark effect. Errors caused by the second source may be reduced when one assumes the shape of the current sheet to be a paraboloidal surface and the line of sight to be in a tangential direction to it. The estimated overall accuracy of the electron density measurement is 30%. Figures 1 and 2 illustrate the radial electron density distribution obtained for Accelerators #5A and #5D, and #1A and #1B, respectively. Both groups of accelerators have the same outer electrode diameters but different inner electrode diameters. In every case, a high electron concentration can be seen near the negative inner electrode, particularly in the case of the Accelerators #5D and #1A where the separations of the two cylindrical electrodes is only 11 mm. It is seen that the density falls off very rapidly toward the outer electrode. With the reversed polarity (positive inner electrode) the density variations are not as steep as for the negative case but are much higher near the outer electrode.

C. Frame and Streak Photographs

The above-mentioned tendency can also be shown qualitatively in the frame and streak photographs obtained. Figures 3 and 4 illustrate frame photographs taken from the

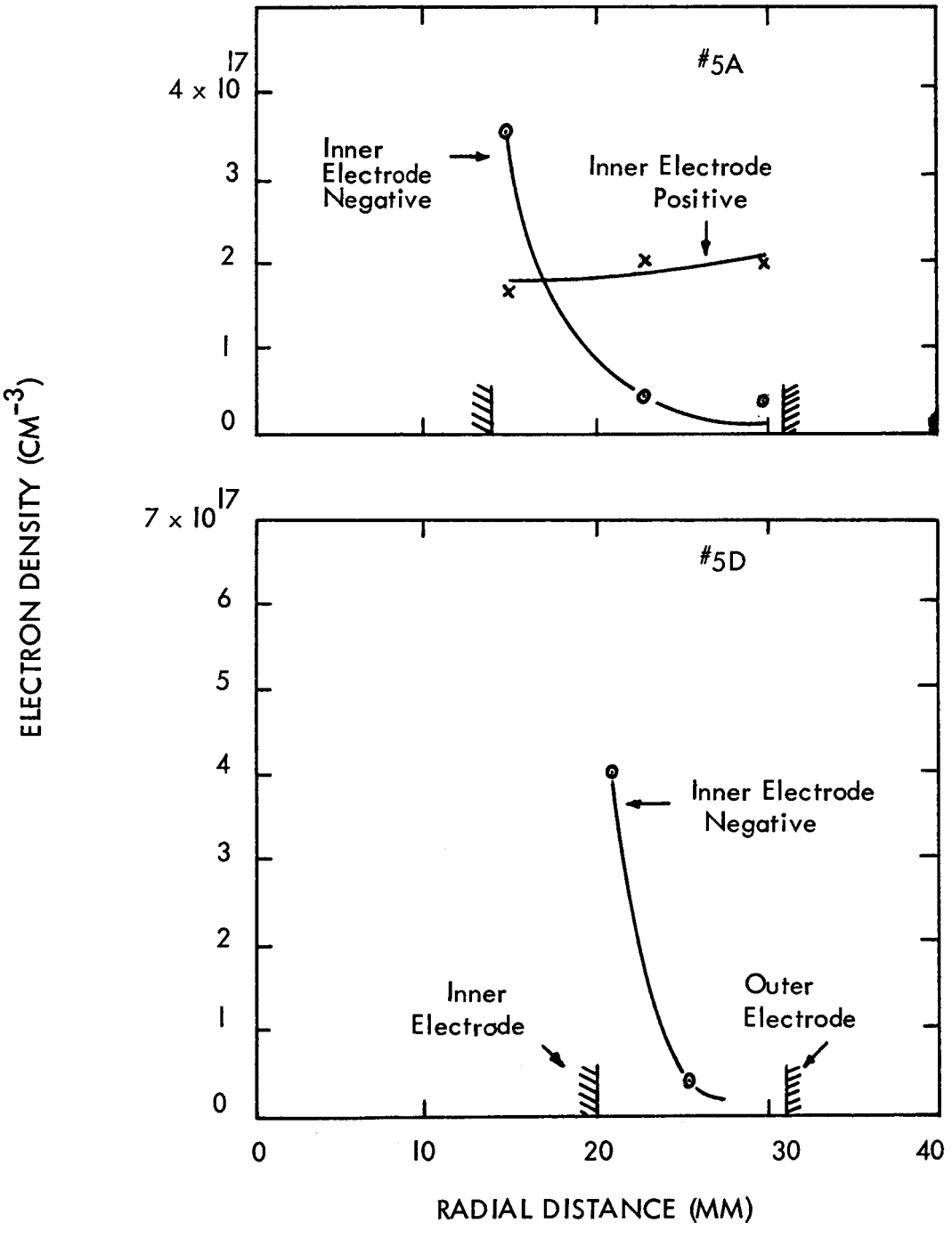

FIG. 1 RADIAL ELECTRON DENSITY DISTRIBUTION OF CURRENT SHEET FOR ACCELERATOR #5A AND #5D

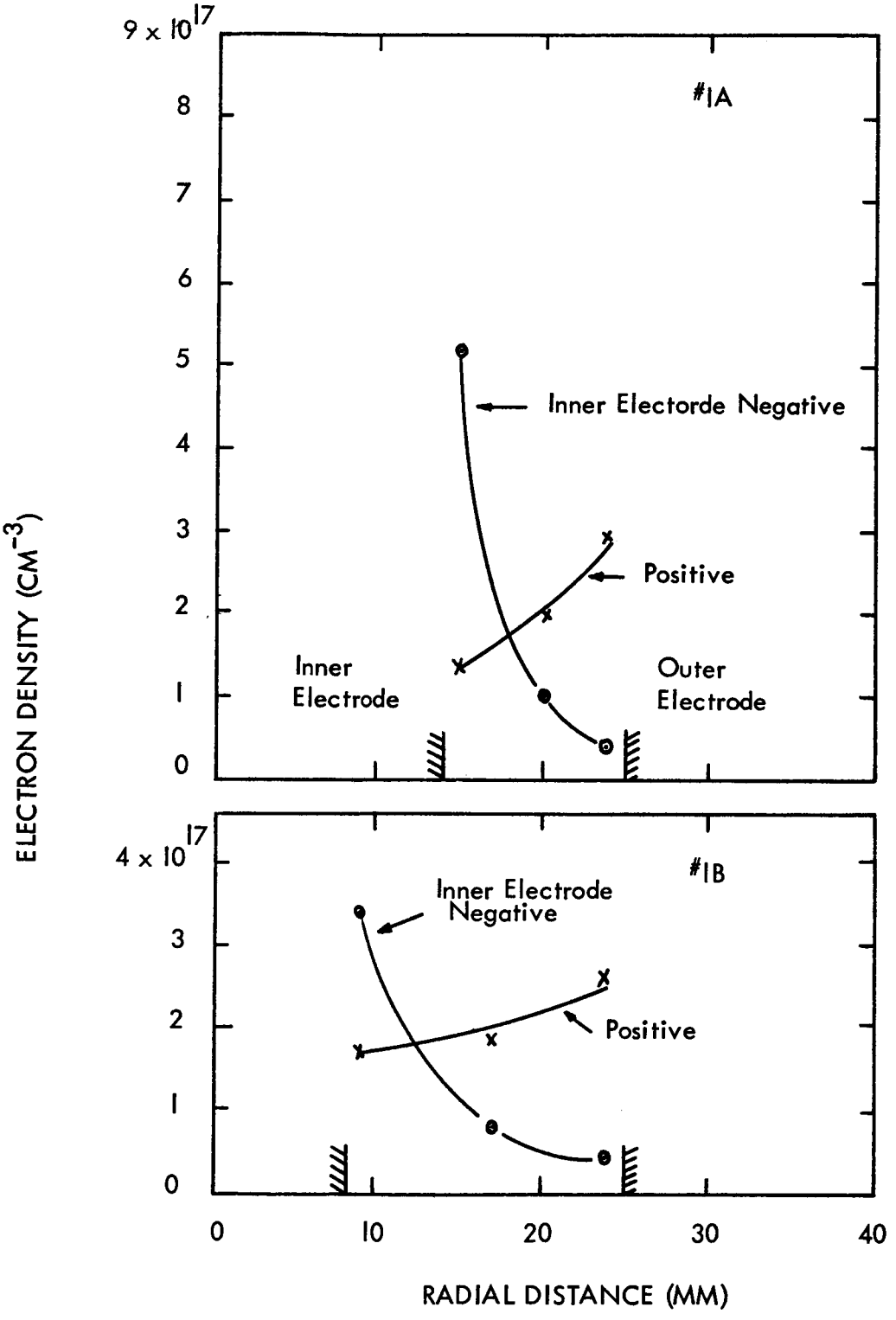

FIG. 2 RADIAL ELECTRON DENSITY DISTRIBUTION OF CURRENT SHEET FOR ACCELERATOR #1A AND #1B

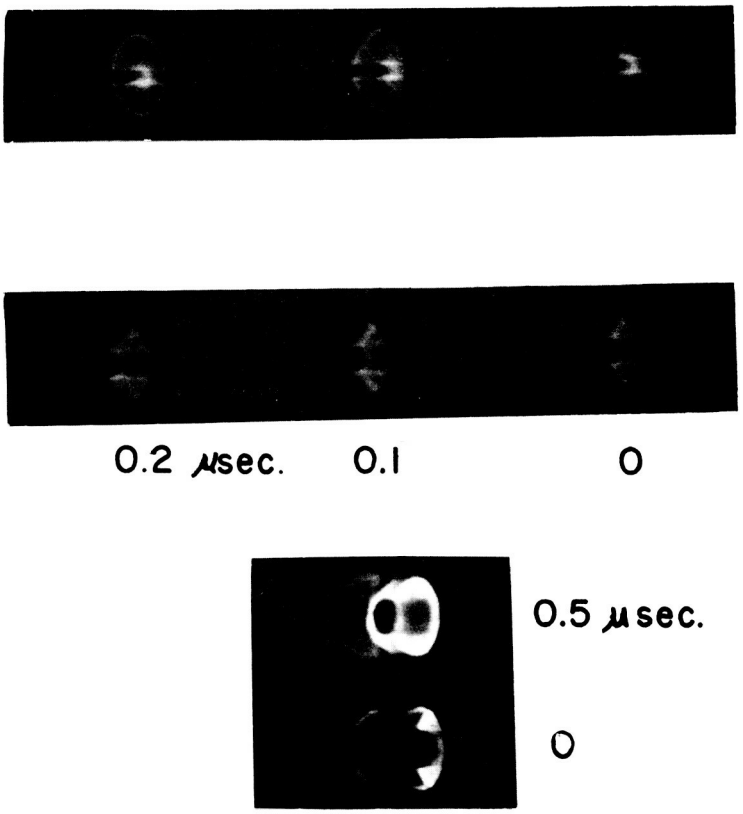

FIG. 3 FRAME PHOTOGRAPHS OF CURRENT SHEET TAKEN AT 45 DEGREES WITH RESPECT TO ACCELERATOR AXIS

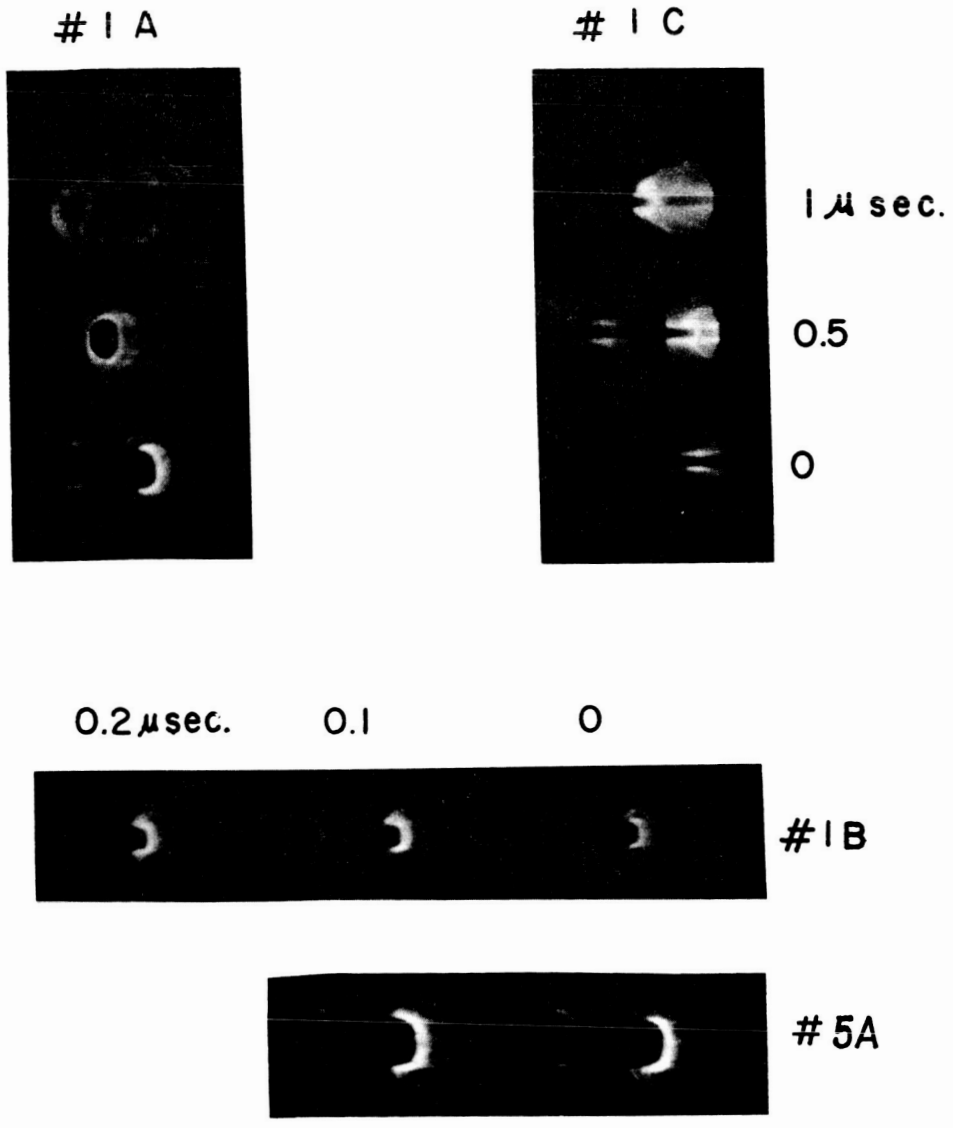

FIG. 4 FRAME PHOTOGRAPHS OF CURRENT SHEET TAKEN AT 45 DEGREES WITH RESPECT TO ACCELERATOR AXIS

direction which is about 45 degrees with respect to the accelerator axis. The faint light front ahead of the main luminosity is a reflected image of the main luminosity at the glass wall. In the case of a negative inner electrode, the luminosity is concentrated mainly on the inner electrode and the remaining portion of the current sheet can hardly be seen. With the positive polarity one can see clearly the paraboloidal shapes of the current sheet with a bright plasma ring at the location where the current sheet intersects the outer electrode. This ring quickly disappears as soon as it detaches from the outer electrode and thus the electron density has a higher value than previous measurements (Figures 1 and 2) which were made at the location 2 mm off the outer electrode. Figure 5 illustrates streak photographs of the luminosity taken with the Coaxial Accelerator #2B which has a slot in its outer electrode. Here again one can see the same tendency, i.e., with the center electrode positive (Figure 5a) the leading front is rather faint and is always accompanied by a bright second front propagating at a much slower velocity, whereas with the reversed polarity the luminosity can be seen only on the first front. The propagation velocity of the first front is about 8 cm/μ sec for both cases and that of the second front which corresponds to the bright ring previously observed in the framing photographs is about 5 cm/μ sec. The electron density distribution dependence on the electric polarity seems to be characterized by a higher electron density in the vicinity of the negative electrode. The higher plasma density near the cathode in the parallel plate plasma accelerator has also been observed by several workers;[3], [5] however, the cause of this phenomena is not well understood. According to Lovberg[3] the entire cathode current is carried by newly formed ions moving into the cathode and the emission of secondary electrons is not likely since 10^4 amperes/cm^2 of electron emission is probably impossible. Present experiments indicate that the electron density near the cathode is even higher for accelerators which have smaller electrode spacing. This problem needs further investigation.

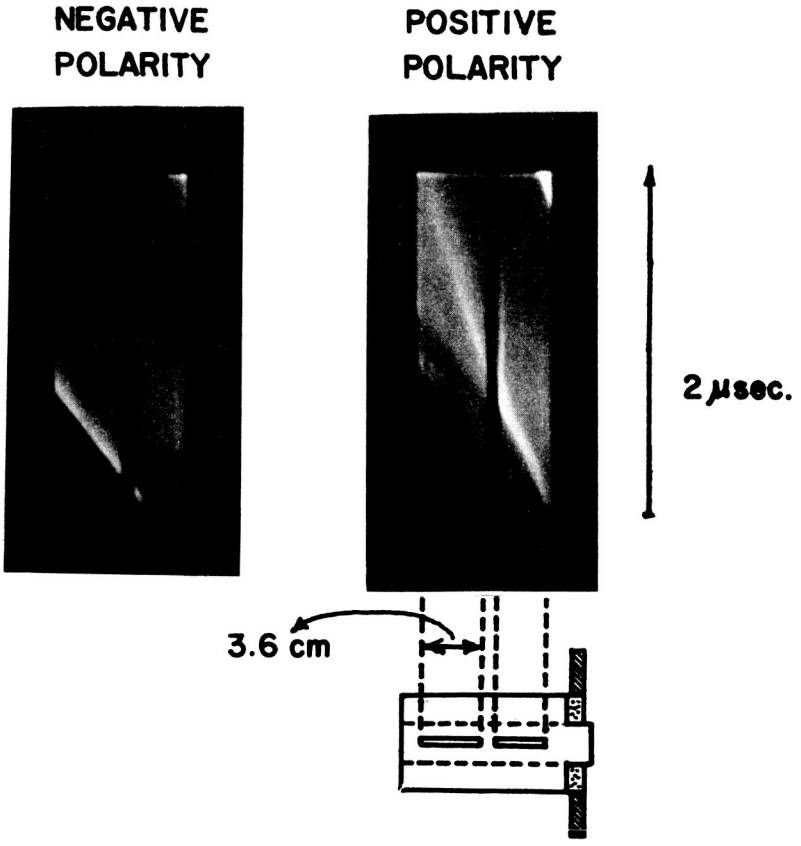

Working gas: Helium at 0.5 Torr
Streak time: 2 μsec

FIG. 5 STREAK PHOTOGRAPHS OF LUMINOSITY TAKEN THROUGH A SLOT ON ACCELERATOR #2B

D. Electron Temperature

Measurement of the electron temperature of the current sheet as a function of radius has been attempted using a technique described in a previous report [7]. According to the discussion in Section IV, the plasma state of the current sheet in the present accelerator is in a condition very close to LTE. Therefore, the error due to the deviation from LTE is small compared with other experimental errors involved. Total intensities of the He II 4686 Å line, the He I 5876 Å line, and the continuum (5210 Å) have been measured simultaneously using a polychromator (modified Czerni-Turner type) with the arrangement shown in Figure 6. The polychromator was calibrated using a tungsten strip-lamp previously calibrated by the National Bureau of Standards. Abel integral inversions for the measured line intensities have not been done here as the shape of the current sheet is more or less paraboloidal and the temperatures do not vary greatly along the line of sight. The result obtained for the Accelerator #IB is shown in Figure 7 where the temperature variations along the radius appear to be small compared with the electron density change (dotted line) for positive polarity operation. The average temperature is 4.2 eV. This is about the same temperature as that obtained for Accelerator #IA [7]. In the case of negative operation, the temperature may be slightly steeper but there exists an uncertainity due to the deviation from LTE because of the low electron density at the midpoint and at the outermost radial position.

E. The Shape of the Current Sheet

There have been some disagreements about the shape of the current sheet in the coaxial plasma accelerators. This may be attributed to the difference in the polarity arrangement and in the type of the working gas used by various workers. This problem was checked qualitatively by taking framing photographs using the image converter camera.

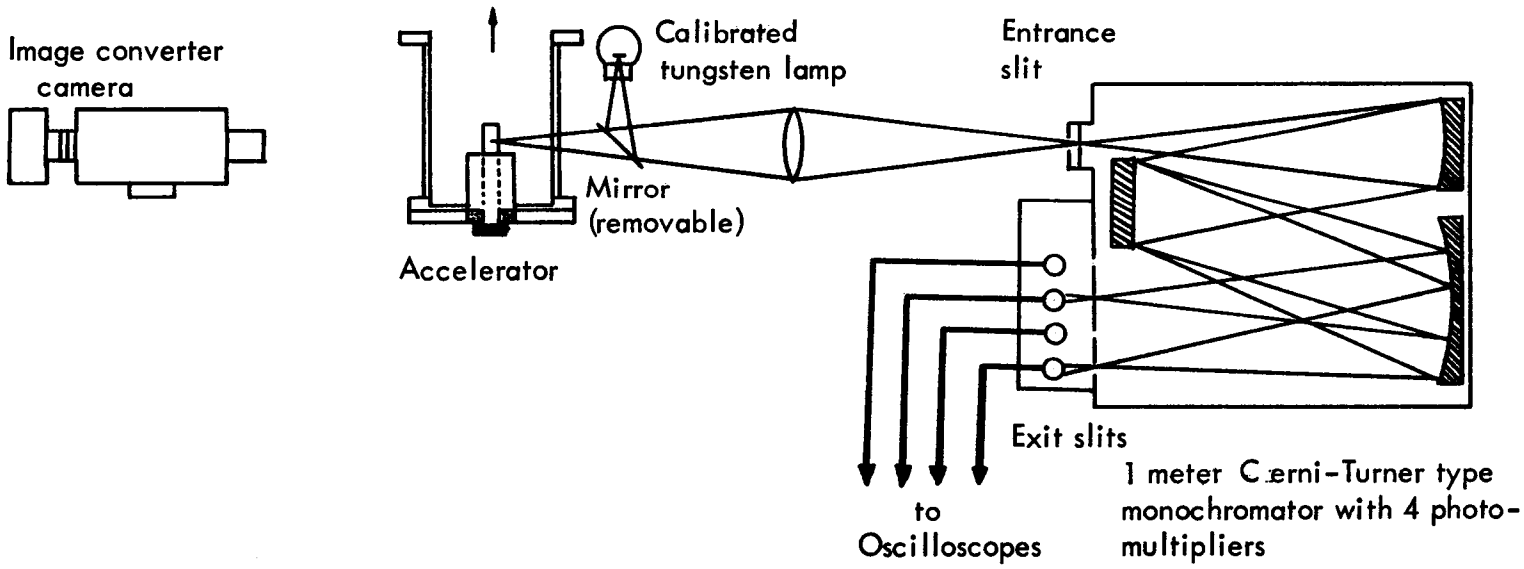

FIG. 6 OPTICAL ARRANGEMENT

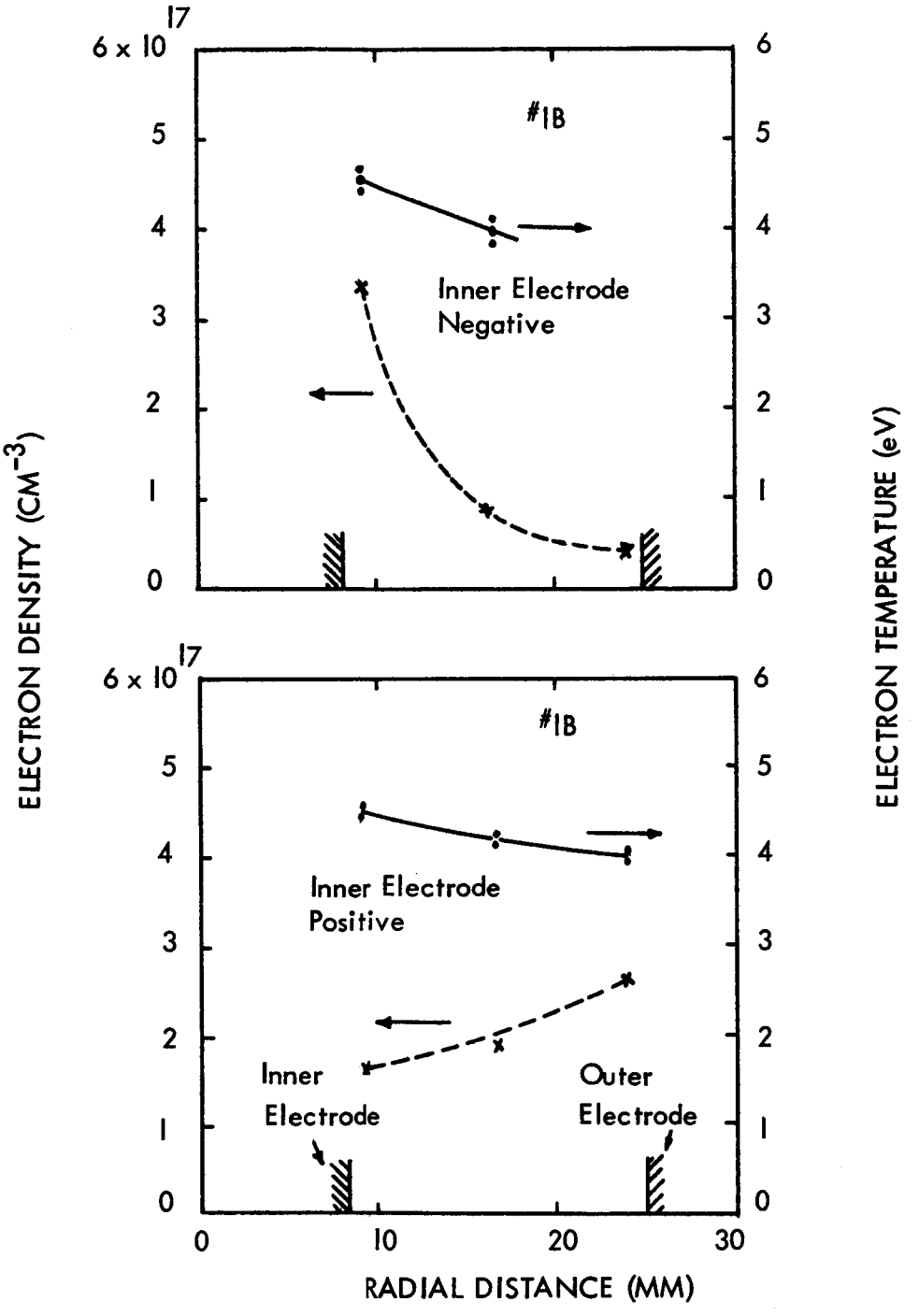

FIG. 7 ELECTRON TEMPERATURE vs RADIUS

Accelerator #IB was operated with both polarities and the tube was filled with hydrogen, nitrogen, argon or helium at pressures which give roughly the same propagation velocity of the current sheet. Figures 8, 9 and 10 show the photographs taken at right angles to the accelerator axis. As can be seen, the polarity dependent behavior of the current sheet in nitrogen and in argon seem to be quite similar to that of helium. The current sheet emerges from the outer electrode with a paraboloidal shape and it pinches toward the axis forming an arrowhead - like configuration in the case of a positive inner electrode. With the reversed polarity (negative inner electrode) the inner electrode surface is covered by a dense plasma sheet and the leading front which is a bright ring around the inner electrode is roughly perpendicular to the electrode surface. In the case of argon, this ring remained unchanged for some time after leaving the inner electrode tip but it is usually destroyed quickly in a disorganized manner.

Figure 11 illustrates frame and streak photographs taken with hydrogen filling. One can also see similar tendencies as for the other gases; however, the difference between the two oppositie polarity cases seems to be much less pronounced (e.g. compare the streak photographs with that in Figure 5) and the shape of the luminous front is paraboloidal for the two cases. In order to check this quantitatively, the radial electron density variation of the current sheet has been determined from absolute continuum intensity measurements at 5210$\mathring{A}$ assuming LTE and a reasonably uniform electron temperature along the radius (which was the case in helium). Figure 12 is the plot of $(Ic)^{1/2}$, which is proportional to the electron density versus radius. The electron density variation in the case of a negative inner electrode is not as steep for hydrogen as helium gas, indicating the polarity dependence on the current sheet in hydrogen is less prominent. This agrees with the previous results obtained for hydrogen by Lovberg [2] and by Mather [8] who observed no polarity effect.

POSITIVE INNER ELECTRODE

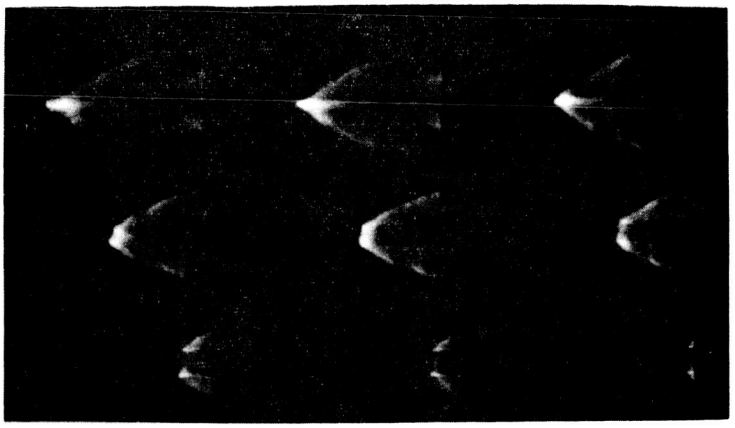

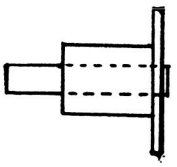

NEGATIVE INNER ELECTRODE

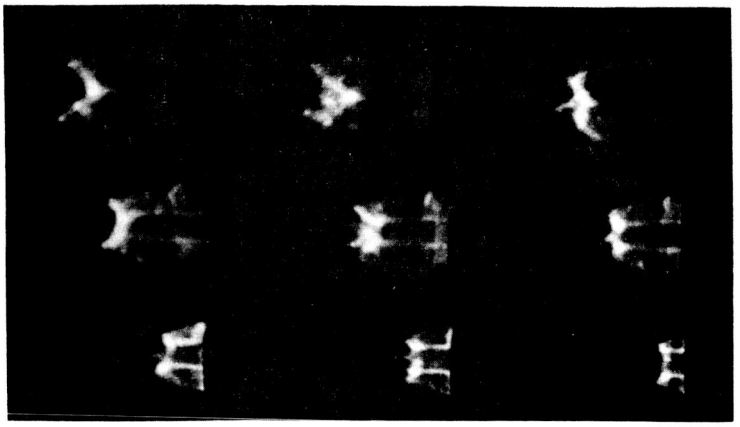

1.2	1.1	1.0
0.7	0.6	0.5
0.2	0.1	0 μ sec.

Accelerator ; #1B
Working gas ; Nitrogen at 0.2 Torr.
Exposure time ; 50 ns.

Fig. 8 FRAME PHOTOGRAPHS OF CURRENT SHEET TAKEN AT A RIGHT ANGLE WITH RESPECT TO THE ACCELERATOR AXIS(NITROGEN)

POSITIVE INNER ELECTRODE

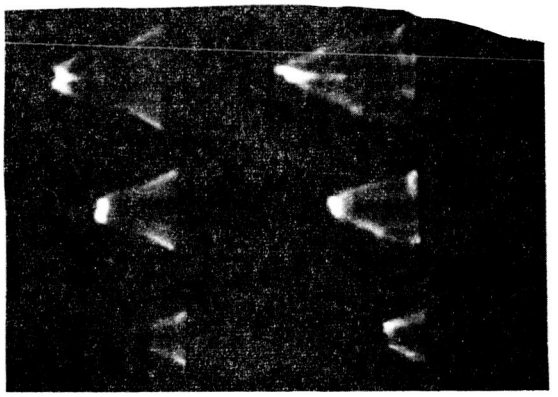

1 μ sec.

0.5

0

NEGATIVE INNER ELECTRODE

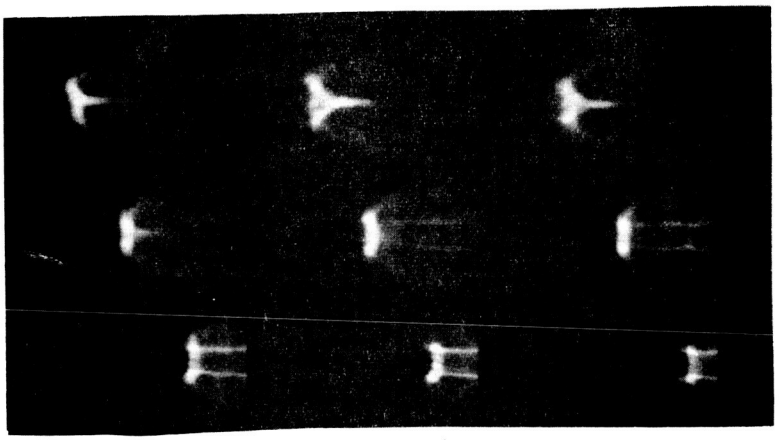

1.2	1.1	1.0
0.8	0.6	0.5
0.2	0.1	0 μ sec.

Accelerator: #1B
Ambient gas: Argon at 0.07 Torr
Exposure time: 50 ns

FIG. 9 FRAME PHOTOGRAPHS OF CURRENT SHEET TAKEN AT A RIGHT ANGLE WITH RESPECT TO THE ACCELERATOR AXIS (ARGON)

POSITIVE INNER ELECTRODE

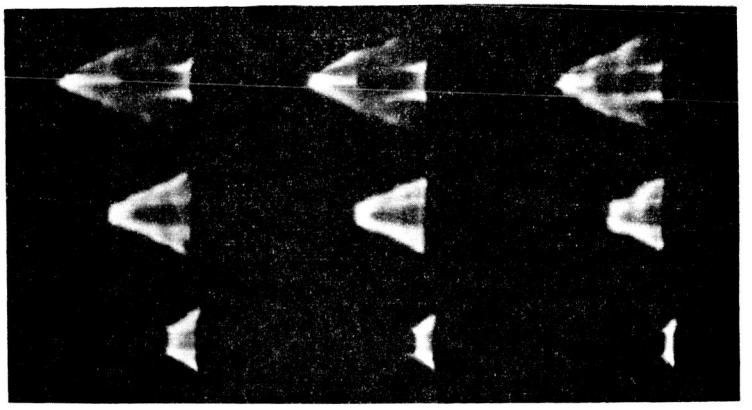

NEGATIVE INNER ELECTRODE

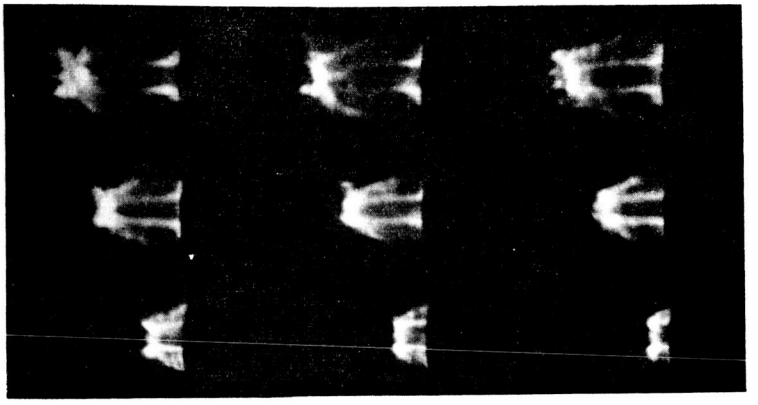

1.2	1.1	1.0
0.7	0.6	0.5
0.2	0.1	0 μ sec.

Accelerator: #1B
Ambient gas: Helium at 0.5 Torr
Exposure time: 50 ns

FIG. 10 FRAME PHOTOGRAPHS OF CURRENT SHEET TAKEN AT A RIGHT ANGLE WITH RESPECT TO THE ACCELERATOR AXIS(HELIUM)

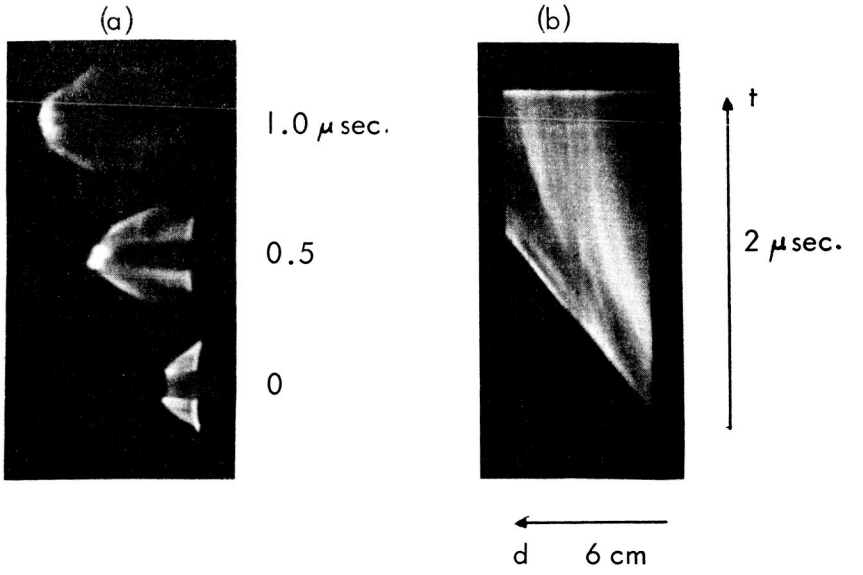

Working gas: Hydrogen at 1 torr
Accelerator: #1B for (a) and (c)
#2B for (b) and (d)

FIG. 11 FRAME AND STREAK PHOTOGRAPHS OF LUMINOSITY IN THE CASE OF HYDROGEN FILLING

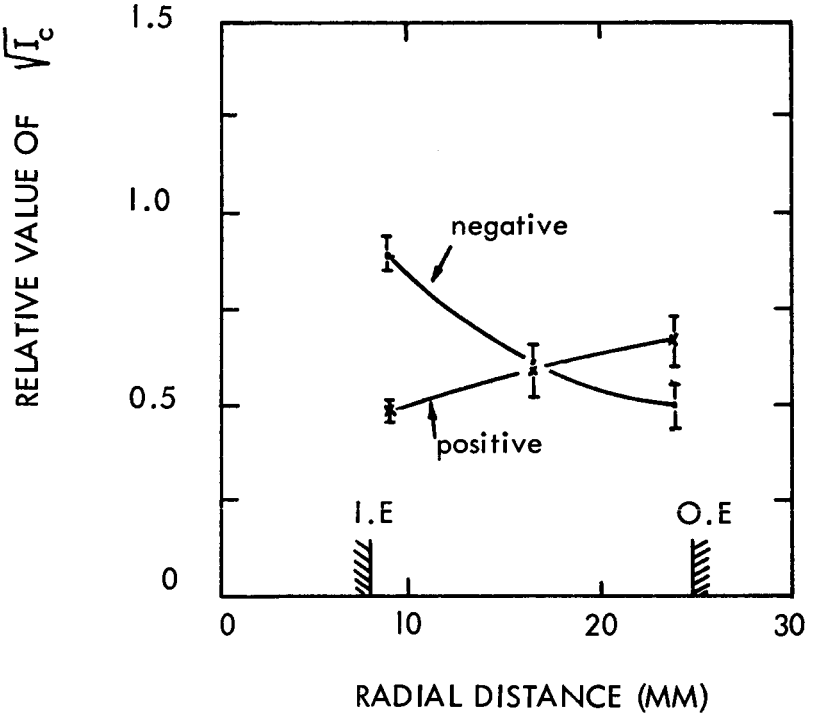

Working Gas : Hydrogen at 0.5 Torr

Accelerator : #1B

FIG. 12 RELATIVE ELECTRON DENSITY IN THE CASE OF HYDROGEN FILLING

The current sheet shapes in the case of negative inner electrode for helium, nitrogen, and argon are not well defined as can be seen in Figures 8, 9, and 10. Higher plasma density near the inner electrode (cathode) may indicate an unusually high current density of the radial component at this location. The rapid drop in the electron density in the remaining part of the annulus then is due to the increase of the current sheet thickness in addition to the radial spreading of the current sheet.

The shapes of the luminous front have been checked using the following experimental arrangement which is shown in Figure 13, i.e., two monochromators were focused at two different annular positions and simultaneous recordings of the He II 4686Å signals were made to compare the arrival time of the signals. Typical oscillograms which are the signals from the innermost and from the outermost radial positions are also shown in Figure 13. In the case of a positive inner electrode, the time delay between the two signals (corresponding to a separation of 2 cm in space) appeared as expected. With the positive polarity, the time delay between the main peak is as long as 0.6 μsec (corresponding to a separation of about 5 cm in space), however, there exists a low lying signal ahead of the main peak in the signal from the outermost position indicating that the luminous front is not canted as for the positive case. Same experiments with the Accelerator #IA show the arrival time of the two signal peaks even coincide in time. It was confirmed that the low lying signal is not scattered light from the plasma near the inner electrode region by checking its line width which is found to be very small.

The models of the current sheet based on the delay of the arrival time at the various annualar positions and based on the framing photographs for gases heavier than hydrogen are shown in Figure 14. It is noteworthy that the both models are rather similar to the early result

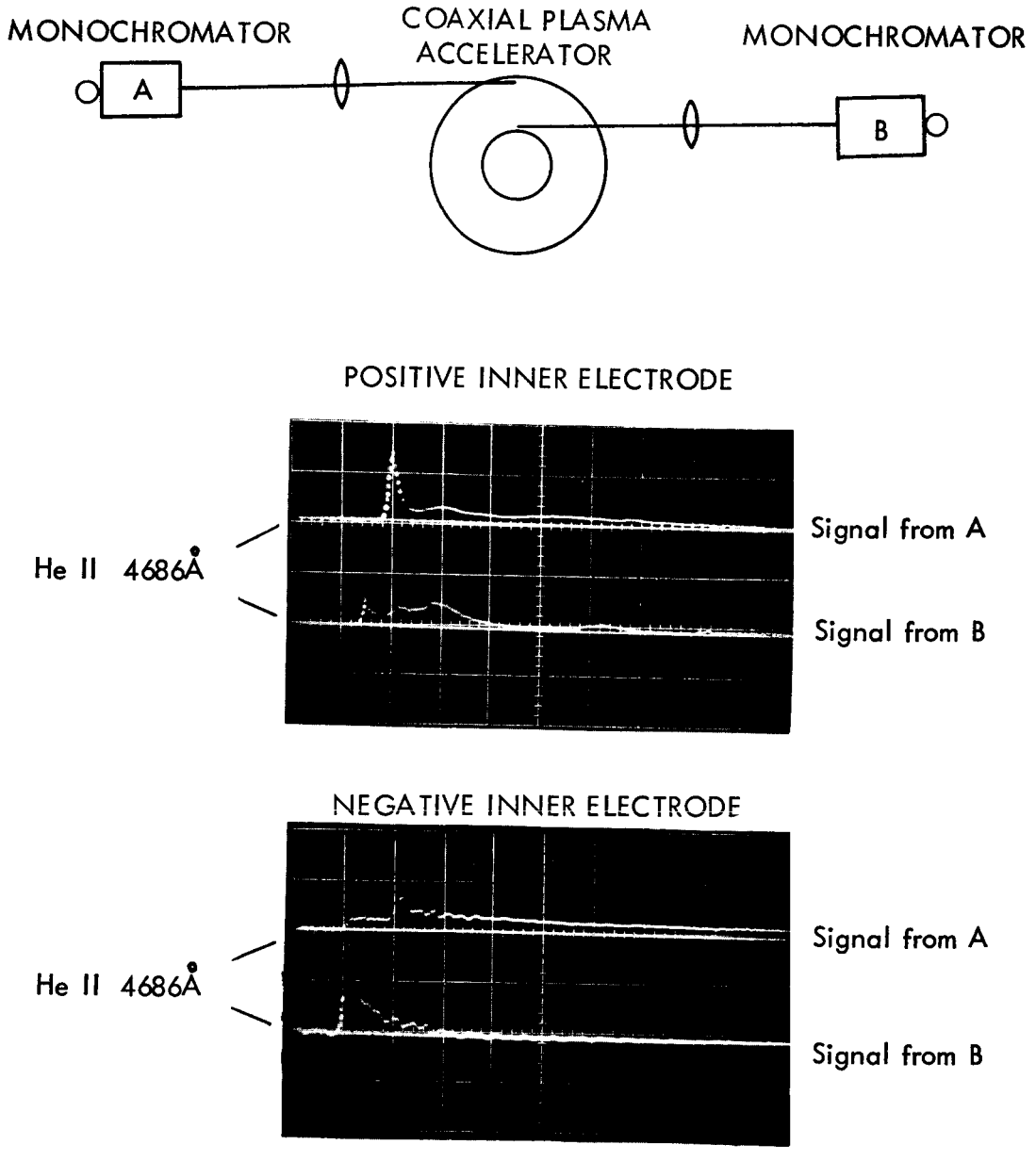

Accelerator ; 1 B
Working gas ; Helium at 0.5 Torr

FIG. 13 SIMULTANEOUS PHOTOELECTRIC RECORDINGS AT TWO DIFFERENT ANNULAR POSITIONS

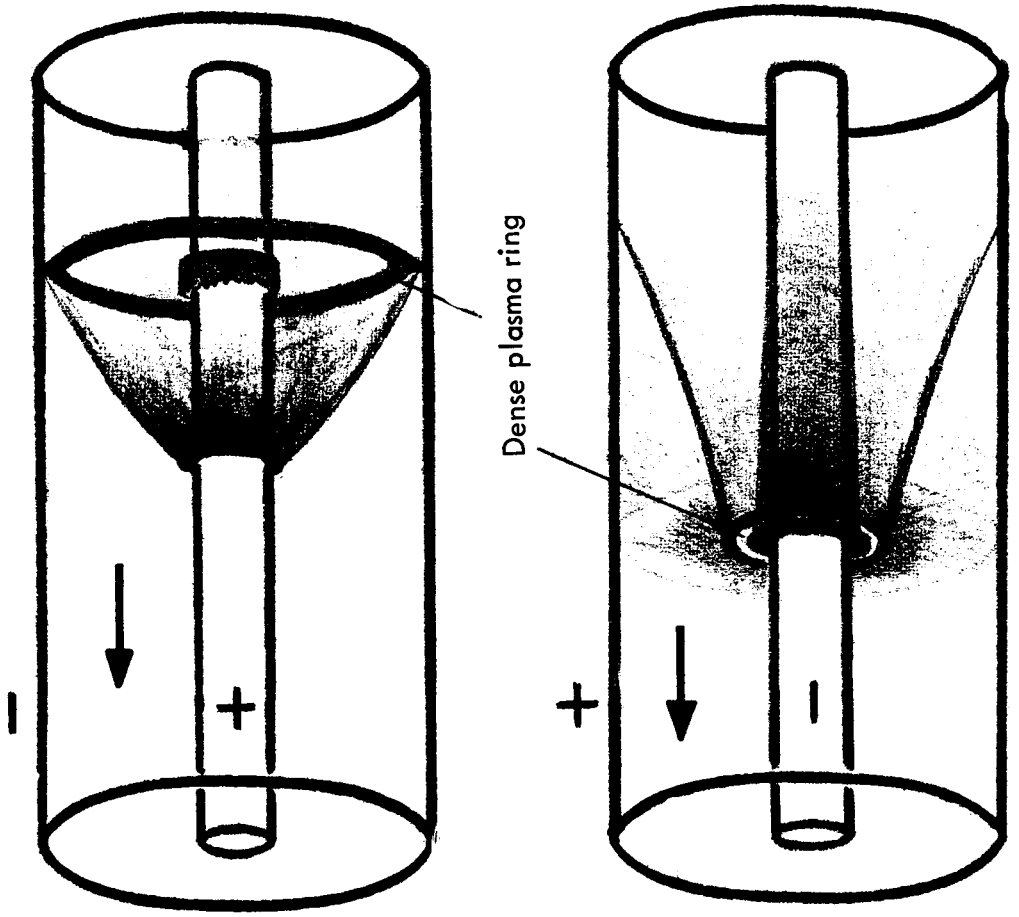

FIG. 14 CURRENT SHEET MODELS

obtained by Keck [1] who used argon and plotted current distributions for positive and negative inner electrodes in a large radius-ratio magnetic annular shock tube.

In summary, the electric polarity effects in the electron density distribution, in the electron temperature, and in the shape of the current sheet have been demonstrated here. The effect is a distinct phenomenon for all accelerator geometries used and for most of the working gases used except hydrogen. In hydrogen, the difference in the shape and the radial electron density between two opposite polarity operations is less noticeable.

III. Preliminary Experiment on Parallel Plate Plasma Accelerator

A. Introduction

The different behavior of the current sheet near the positive and the negative electrode in a parallel plate plasma accelerator has been observed by several workers [3], [4], [5] although a reasonable explanation of this phenomenon is still not available. Polarity dependent phenomena in a coaxial accelerator described in the previous section seem to be essentially the same as those which takes place in a parallel plate plasma accelerator. The current sheet in a coaxial accelerator is influenced by the non-uniform magnetic field along the annulus behind the current sheet but in addition to this influence, a similar process as in the parallel plate accelerator also is taking place. This is understandable if one examines Figure 14 in this report and also Figure 3 of reference 1. The main purpose of this study is to investigate the physical process which takes place near the electrode region and which controls the gross behavior of the current sheet. The advantage of the parallel plate geometry over the coaxial accelerator is the simple convenience in making the spectroscopic measurements, particularly the observation near the electrode region. Also, one can choose a line of sight for the measurement along which the plasma properties are roughtly uniform. The other advantage is that one can exclude the influence due to the non-uniform B_θ field as in the coaxial geometry.

Only preliminary experimental results on the parallel plate accelerator are presented here; however, quantitative measurements are underway.

B. Gross Structure of the Current Sheet

Schematic diagram of the accelerator is shown in Figure 15. A pair of copper plates 6 cm wide, 8 cm long and 3.5 cm apart were enclosed by a quartz tube of 6 inches diameter. The discharge was driven by a 15 F capacitor charged to 10 kV and triggered by a pressurized switch. The ringing frequency is about 130 kc/s. The vacuum system had a liquid nitrogen cold trap and the base pressure was 6×10^{-7} Torr.

Figure 16a shows framing photographs of the discharge produced in helium at a pressure of 0.5 Torr. The photographs were taken from the side and one can see well-known features of the current sheet, i.e., an instability begins to develop near the positive electrode and the current sheet tilts as a whole at a late stage of the discharge. The cathode surface is covered by thin sheets of dense plasma as has been reported.[3], [5] However, besides this behavior one may notice a bright spot within the current sheet formed briefly at the middle of the electrode gap. This node-like spot appears to be a location where some of the divided current paths join to form a single path. Figure 16b shows an end-on view of the current sheet. It can be seen that a bright zone parallel to the magnetic field advances upward and it finally reaches the cathode forming a high plasma density region. It should be noted that the higher electron density observed in the vicinity of the negative electrode in a coaxial accelerator may also be caused by a similar process as described here. However, it has to be confirmed by measuring the electron densities at the appropriate locations.

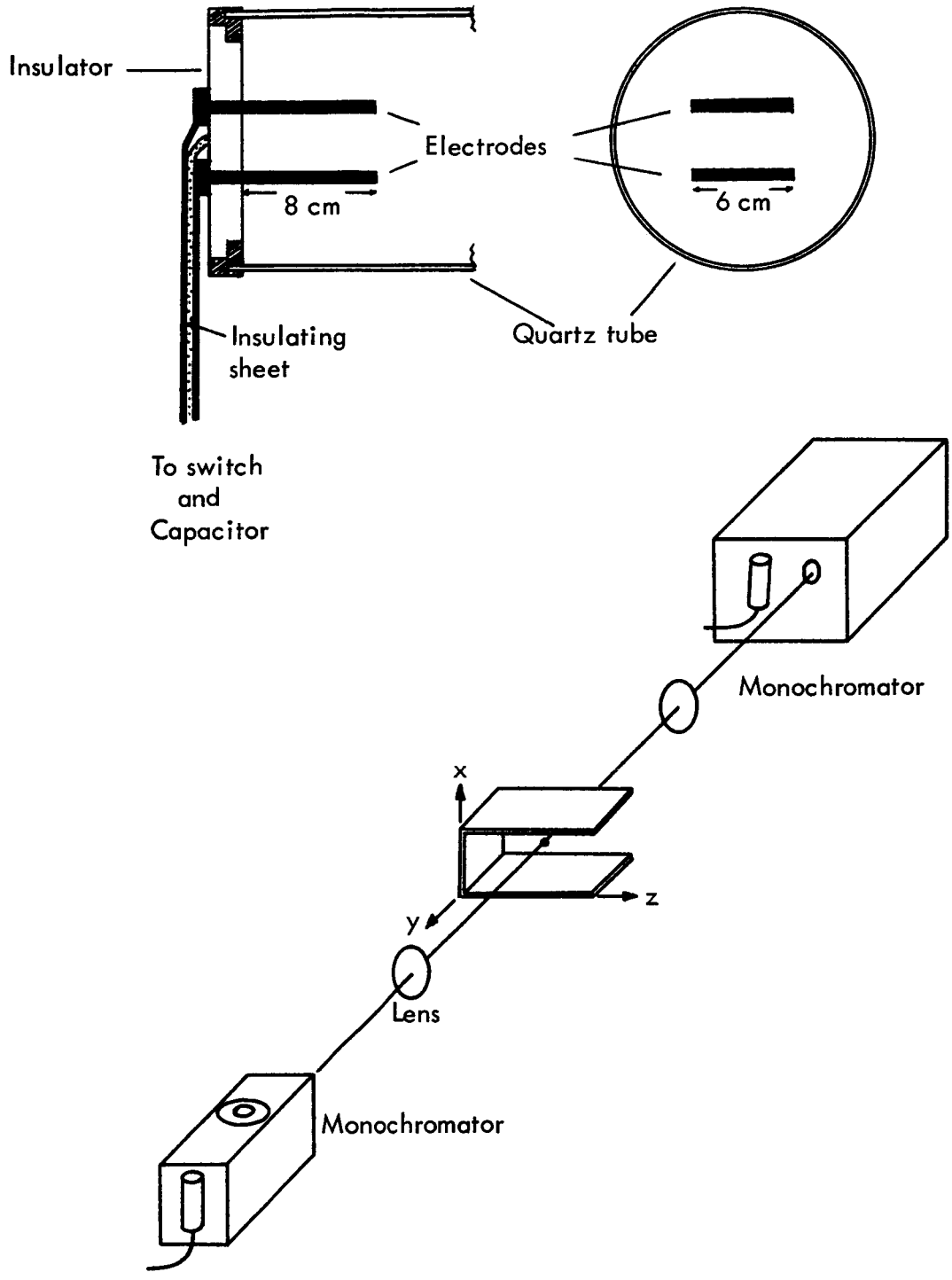

FIG. 15 SCHEMATIC DIAGRAM OF PARALLEL PLATE PLASMA ACCELERATOR AND OPTICAL ARRANGEMENT

(a)

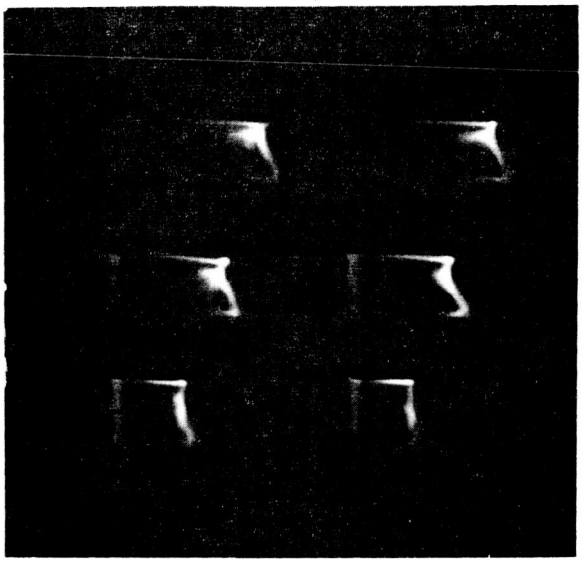

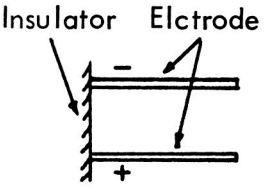

2.0 1.8

1.5 1.3

1.0 0.8 μ sec .

(b)

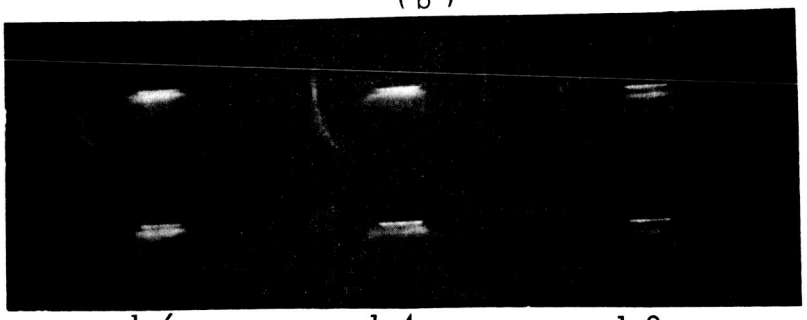

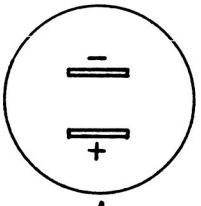

Vacuum chamber wall

1.6 1.4 1.2

1.1 0.9 0.7 μ sec .

Working gas ; Helium
Exposure time ; 50 ns .

FIG. 16 FRAME PHOTOGRAPHS OF DISCHAGE TAKEN FROM THE SIDE (a) AND FROM THE END OF THE ACCELERATOR(b)

C. Photoelectric Signals

The plasma radiation emitted by a propagating current sheet was observed using the optical arrangement shown in Figure 15. Two monochromators were aligned to the same optical axis (the direction of the y-axis in Figure 15). The precise alignement was confirmed each time by comparing the two photoelectric signals recorded simultaneously by two monochromators which were both set at the He II 4686Å line. It was found that the signals along a fixed line of sight are fairly reproducible for an extended period of time until the electrodes become dirty. The line of sight was fixed in the x-y plane at z=4 cm and the observations were made at several locations along the x-axis. The simultaneous recordings of the He II 4686Å and the other lines under investigation, including that of the impurities indicate unexpectedly high precursor radiations (or pre-breakdown plasma) ahead of the main current sheet. In fact, the current sheet is by no means well defined in this sense as had been thought previously. The signal shapes and the time correlation between the various lines are different at the cathode, at the anode, and at the remaining parts of the electrode gap. Figure 17 illustrates typical oscillograms obtained. The similar precursor signal of the impurity lines were also previously observed in the coaxial plasma accelerators.(7) Further investigations and analysis are under progress.

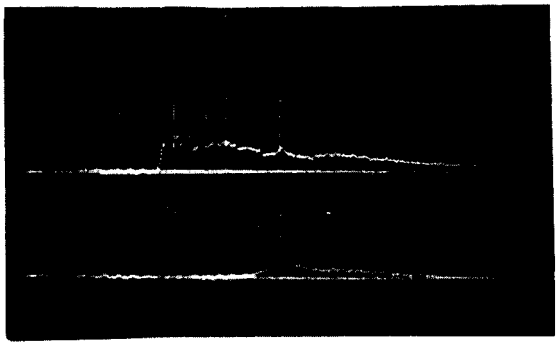

Z = 4 cm, $\dot{X}$ = 3.3 cm

(2 mm off the anode)

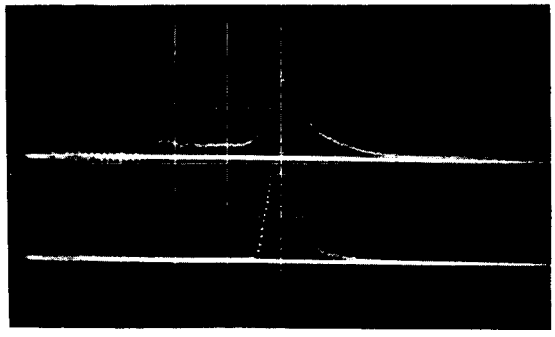

Z = 4 cm , X = 1.7 cm

(midpoint of the electrode gap)

0.5 μ sec/div

FIG. 17 Typical Oscillagrams of Photoelectric Signals

IV. Validity of the LTE Assumption - Spectroscopic Analysis

A. Introduction

In this investigation, the electron density, the electron temperature and the composition of the plasma are obtained from spectroscopic analysis. However, controversy still surrounds the interpretation of spectroscopic data obtained with various types of electric shock tubes. The controversy centers on whether or not local thermodynamic equilibrium (LTE) exists in such plasmas during the course of investigation. Therefore, the validity of our conclusion concerning the macroscopic plasma behavior depends on the resolution of this point.

Costa and Tondello[9] have made extensive measurements of helium line and continuum intensities and line widths in the plasma produced by a conical pinch discharge. They found that a self-consistent temperature of 4 eV and an electron density of $\sim 10^{17}$ cm^{-3} was obtained using the LTE assumption. Earlier McLean, et. al.[10] and Wiese, et. al.[11], and Berg et. al.[12] made studies of helium shock waves in a T-tube with essential agreement between their experiments.

However, Isler and Kerr[13] and Eckerle and McWhirter[14] have re-examined the LTE assumption and alledge that LTE does not exist in either a conical z-pinch, He-filled, shock tube or in a T-tube containing 99% H_2 and 1% He mixture. In all these experiments, the electron density (as measured from line widths or absolute continuum intensity) was in the 10^{17} cm^{-3} range.

The Isler - Kerr[13] and Eckerle - McWhirter[14] results are in gross disagreement. Isler - Kerr claim that the density of doubly - ionized helium is as much as five orders of magnitude higher than would correspond to LTE, while the Eckerle - McWhirter data analysis yields population numbers that are much lower than expected for LTE.

Since the LTE is central, the collisional and radiation processes which determine the bound state and ionic population must be considered, as will be seen later, and it is concluded that the LTE assumption is in fact a satisfactory approximation for conditions of these experiments.

B. Validity of LTE Assumption

Let us consider a helium plasma with a high degree of single ionization so that the predominant population belongs to He II. The electron density, which is found from observations and which does not depend on the LTE assumption, is in the 10^{17} cm^{-3} range. In such a plasma, either in pure helium or in a He - H_2 mixture, collisional - radiative calculation[15] show that the bound states of He I are in Saha - Boltzmann equilibrium and also the ground state population of He I is in LTE with the ground state of He II. The controversy arises in connection with the population of excited He II and the number of He III ions, relative to the ground state population of He II.

(1) Relative population of He III and excited states of He II

Knowing the electron density and assuming a value for the electron temperature one can[15], [16] determine the lowest quantum level whose population is in LTE with the populations of the higher discrete levels and with the distribution of the free electrons. This quantum level lies between n=2 and n=3 for singly-ionized helium when $N_e \sim 1\text{-}2 \times 10^{17}$ cm^{-3} and T is within a factor 2 of 5 eV. Thus, for $n>2$, the bound states of He II and the population of He III can be related by Saha - Boltzmann relations.

(2) Intensity of He II spectral lines

One is ultimately interested in relating spectral intensities of optically thin lines to the local electron temperature. The line intensity is given by

the usual formula

$$I_{mn}^{o,+} = \hbar \omega_{mn}^{o,+} A_{mn}^{o,+} N_m^{o,+}, \tag{1}$$

where o, + refer to He I and He II and m and n are the upper and the lower levels of the line, respectively. For He I

$$N_m^o = N_1^o \frac{g_m^o}{g_1^o} e^{-\frac{E_m^o}{kT}} . \tag{2}$$

However, for He II one cannot relate N_m^+ ($m \geq 2$) with the ground state population N_1^+ without further justification. However, one can relate N_m^+ to N_2^+

$$N_m^+ = \frac{g_m^+}{g_2^+} N_2^+ e^{-\frac{E_{m2}}{kT}}, \tag{3}$$

Where $$E_m^+ - E_2^+ = E_{m2}^+$$

Thus
$$I_{mn}^o = \left[\hbar \omega_{mn}^o A_{mn}^o \frac{g_m^o}{g_1^o} e^{-\frac{E_m^o}{kT}} \right] N_1^o \tag{4a}$$
$$\equiv F^o(T) N_1^o$$

and
$$I_{mn}^+ = \left[\hbar \omega_{mn}^+ A_{mn}^+ \frac{g_m^+}{g_2^+} e^{-\frac{E_{m2}^+}{kT}} \right] N_2^+ \tag{4b}$$
$$\equiv F^+(T) N_2^+$$

The line ratio is accordingly

$$\frac{I_{mn}^+}{I_{mn}^o} = \frac{F^+(T)}{F^o(T)} \cdot \frac{N_2^+}{N_1^o} . \tag{5}$$

In the case of complete LTE

$$(N_2^+) = N_1^+ \left(\frac{g_2^+}{g_1^+}\right) e^{-\frac{E_{21}^+}{kT}} \tag{6}$$

and

$$\frac{N_1^+}{N_1^o} = \frac{S(T)}{N_e} \tag{7}$$

where N_e is the electron density and S(T) is the familiar Saha function. Using Equations (6), (7) and (5) one obtains

$$\left(\frac{I_{mn}^+}{I_{mn}^o}\right)_{LTE} = \frac{F^+(T)}{F^o(T)} \left(\frac{g_2^+}{g_1^+}\right) e^{-\frac{E_{21}^+}{kT}} \frac{S(T)}{N_e}$$

$$= \frac{4}{N_e} \frac{F^+(T)}{F^o(T)} \cdot S(T)\, e^{-\frac{E_{21}^+}{kT}} \tag{8}$$

Knowing N_e and the intensity ratio, one can obtain a temperature in the usual (and controversial) way. A similar analysis follows for the determination of temperature from line/continuum ratios.

Suppose now that an extreme non LTE situation exists, i.e., the radiative decay rate in He II from n=2→1 is much greater than the corresponding collisional de-excitation rate.

In that case, for the steady state optically thin case one can write

$$A^{+}_{21}\,(N^{+}_{2})_c = \langle \sigma^{+}_{12}\, V \rangle\, Ne\, N^{+}_{1}\ , \qquad (9)$$

where the subscript c denotes this "corona" approximation and following Seaton [17] the collisional excitation rate coefficient is

$$\langle \sigma^{+}_{12}\, V \rangle = \frac{6 \times 10^{-6} f^{+}_{12}}{E^{+}_{12}\sqrt{T_e}}\, e^{-\frac{E^{+}_{12}}{KT}} \qquad (10)$$

where E^{+}_{12} and T_e are in units of eV, $f^{+}_{12} = 0.4$ is the absorption oscillator strength corresponding to the transition probability $A^{+}_{12} = 7.4 \times 10^{9}\ sec^{-1}$. If we now use (8), (6) and (5) we obtain

$$\left(\frac{I^{+}_{mn}}{I^{o}_{mn}}\right)_c = \frac{F^{+}(T)}{F^{o}(T)}\,\frac{\langle \sigma^{+}_{12}\, V \rangle\, Ne\, N^{+}_{1}}{A^{+}_{21}\ N^{o}_{1}}$$

$$= \frac{F^{+}(T)}{F^{o}(T)}\,\frac{\langle \sigma^{+}_{12}\, V \rangle}{A^{+}_{21}}\, S(T) \qquad (11)$$

$$= \frac{8 \times 10^{-18}}{\sqrt{T_e}}\left[\frac{F^{+}(T)}{F^{o}(T)}\, e^{-\frac{E_{12}}{KT}} \cdot S(T)\right]$$

Comparing (8) and (11) shows that for $N_e \sim 10^{18}$ cm^{-3}, with $T_e \sim 4$ eV, the corona and LTE approximations yield the same result. However, for $N_e = 1.4 \times 10^{17}$ cm^{-3}, which is the density measured in this experiment, a difference is expected in the temperature as calculated using the appropriate LTE and corona formulas. For example, using a typical ratio of He II 4686 Å to He I 5876 Å line intensities of $3.27 \pm 20\%$, the LTE relation gives $T_e = 4.0 \pm 0.1$ eV and the corona relation gives $T_e = 4.5 \pm 0.1$ eV, where the uncertainty in the temperatures reflects only the experimental errors. The corona temperature is noted to be only 11% higher than the LTE temperature. Thus, we agree with the statement that purely spectroscopic measurements of the type discussed will hardly establish that collision-dominated LTE exists. A self-consistent picture can be obtained using either approximation. This argument along casts suspicion on claims that very large departures from LTE temperatures occur (13), (14). To deal further with this question, relaxation times and opacity must be estimated.

(3) Opacity of the He II resonance line

If the resonance line of He II is optically thick, then absorption and remission reduces the probability that the photons escape by a factor equal to the mean number of photon reabsorptions. In this way, the effective life time of the excited level is increased proportionately, e.g., see References 18 and 19.

For helium shocks, where $N_e \approx N_1^+$, the optical depth $(k_o \cdot d) \sim 100\text{-}1000$. This reduces the radiative decay rate, R_{rad}, considerably i.e.,

$$R_{rad} \approx \frac{A_{21}^+}{(k_o \cdot d)} \sim 10^7 \text{ sec}^{-1} \qquad (12)$$

Comparing this rate with the collisional de-excitation rate, one has

$$R_{coll.} \sim \frac{6 \times 10^{-6} f_{12}^{+} N_e g_1}{E_{12}^{+} \sqrt{T_e}\, g_2} \sim 10^{9}\ sec^{-1} \qquad (13)$$

Thus, self-absorption causes collisional de-excitation to be much more important than the corresponding process of radiative decay, and it can be concluded that in the steady state the corona approximation does not apply to the plasma of interest. The strong self-absorption tends to equilibrate the n = 1 and 2 levels of He II, making the "apparent" temperature closer to the LTE value predicted by Eq. (8) rather than the corona Eq. (11)

(4) Relaxation Effects

In order to establish whether the population numbers of He II approach their steady state value, the time constants for collisional excitation and radiative-collisional de-excitation must be considered. The characteristic relaxation time for exciting the n = 2 level $\left[\langle \sigma_{12}^{+} v \rangle N_e\right]^{-1}$ is $\sim 2 \times 10^{-6}$ sec. However, it must also be considered that only a fraction of the ground state ions need be excited, which will be of the order of the fractional ionization to He III, i.e., $N^{++}/N^{+} \approx 0.1$ (see Eq. 6-65 of Reference 20). The estimated relaxation time is thus $\sim 0.2\,\mu$ sec and is therefore comparable to experimental times. This suggests that approximate LTE extends down to the ground state of the ion.

Eckerle-McWhirter and Isler-Kerr argued that the recombination rate is too small for the plasma to follow rapid changes in the temperature. However, the temperature determined by E-M from the Balmer discontinuity is probably high by a factor of about two because the contribution of the Balmer line wings (especially from the dense boundary layer)

was not taken into account (16). It should be noted that if the E-M data is analyzed with the LTE assumption, then the results are consistent experiments of References 9 - 12. If the data is analyzed with a wrong temperature, then there is a large discrepancy with LTE. It is clear that E-M have not shown that there is a drastic departure from LTE.

Isler and Kerr argue that in a rapidly cooling plasma behind the luminous front, the recombination rate is as long as 1μ sec. We accept their model that $m \geq 3$ levels are in equilibrium with He III ions and free electrons, but seem to disagree with their estimates of the time required to fill the ground state from $m \geq 3$. For their conditions, $N_3^+ \approx 2 \times 10^{-3} N^{++}$. Now, the transition probability for the Balmer line of He II is about $A^+_{32} \sim 0.5 \times 10^9$ sec^{-1}, the decay rate from N^{++} to N_3^+ to N_2^+ is at least $N_3^+ A^+_{32} \sim 10^6 N^{++}$ cm^{-3} sec^{-1}, (level 3 will be filled from above at a still faster rate). Also, one should consider radiative decay from the continuum and from $n > 3$. These also contribute about $10^6 N^{++}$ cm^{-3} sec^{-1} to the recombination rate, even if direct transitions to the ground state are ignored. Finally, collisional de-excitation from $3 \rightarrow 2$ is also important and will increase the recombination rate. With electron densities between $(3\text{-}10) \times 10^{16}$ cm^{-3}, this rate is $(2\text{-}6) \times 10^9 N_3^+ \approx (0.4 - 1) \times 10^7 N^{++}$. Thus the total collisional-radiative recombination rate to n=2 would be $(5\text{-}10) \times 10^6 N^{++}$ cm^{-3} sec^{-1}.

The refilling of the upper levels from n=2 level will not decrease this recombination rate because the reverse processes will only become significant when N_2^+ approaches its LTE value, i.e., $(N_2^+)_{LTE} \simeq 5 \times 10^{-3} N^{++} - 1.5 \times 10^{-2} N^{++}$ for the temperatures discussed by I-K. With collisional decay rates of $\sim 10^9 N_2^+$ cm^{-3} sec^{-1} (see Equation 13), the total $n=2 \rightarrow 1$ decay rate would then be of the order $(5 \times 10^6 - 1.5 \times 10^7) \times N^{++}$ cm^{-3} sec^{-1}. This rate is

as fast as the filling rate of level 2. Thus the net combination rate

$$\frac{dN^{++}}{dt} \sim 5 \times 10^{6} N^{++} \equiv \frac{N^{++}}{\tau}$$

leads to a relaxation time $\tau \simeq 0.2 \mu$ sec., which is of the same order as the estimated excitation-relaxation time.

Such fast decay times have been observed in numerous experiments including the present experiment. The I-K conclusions are based experimentally mainly on a second peak (in time) of the He II 4686 line, i.e., a phenomena behind the luminous front. This anomaly is not generally observed except when impurities follow the front. That this explains the discrepancy in the I-K experiment and leads to the unbelievable departure of as much as 10^{5} from LTE is still a conjecture.

REFERENCES

1. J. C. Keck, Phys. Fluids 5, 630 (1962).
2. R. H. Lovberg, Phys. Fluids 8, 177 (1965).
3. R. H. Lovberg, Inst. Electron. Trans. Nucl. Sci., NS-11, 187 (1964).
4. R. B. Johansson, Phys. Fluids 8, 866 (1965).
5. J. R. MacLelland et.al., Phys. Fluids 9, 1613 (1966).
6. H. R. Griem and K. Y. Shen, Phys. Rev., 122, 1490 (1961 a).
7. T. N. Lie, A. W. Ali, E. A. McLean and C. C. Chang, 1st Semi-Annual Progress Report, Research Grant NGR-09-005-025, 1966.
8. Private Communication.
9. S. Costa and G. Tondello, Ricerca Sci. 35, (II-A) 949 (1965).
10. E. A. McLean, C. E. Faneuff, A. C. Kolb and H. R. Griem, Phys. Fluids 3, 843 (1961).
11. W. Wiese, H. F. Berg, and H. R. Griem, Phys. Rev. 120, 1079 (1960).
12. H. F. Berg. A. W. Ali, R. Lincke and H. R. Griem Phys. Rev. 125, 199 (1962).
13. R. C. Isler and D. E. Kerr, Phys. Fluids 8, 1176 (1965).
14. K. K. Eckerle and R. W. P. McWhirter, Phys. Fluids 9, 81 (1966).
15. D. R. Bates, A. E. Kingston and R. W. P. McWhirter, Proc. Roy. Soc. (London) A267, 297 (1962).
16. A 20% error in the intensity ratio leads to a factor of 2 error in temperature (See Figure 4 of Reference 14).

17. M. J. Seaton, Atomic and Molecular Processes, edited by D. R. Bates (Academic Press, Inc. New York, 1962).

18. T. Holstein, Phys. Rev. 72, 1212 (1947).

19. A. C. Kolb and R. W. P. McWhirter, Phys. Fluids 7, 519 (1964).

20. H. R. Greim, Plasma Spectroscopy (McGraw-Hill Book Company, New York 1964).